RFinder: Pinpoint the Invisible RFID Tags in the Prefabricated Buildings

Jiacheng Zhang[1], Meng Jin[2], Yimiao Sun[1], Weiguo Wang[1], Jia Zhang[1], Xin Na[1], Xiuzhen Guo[3], Yuan He[1*]
[1]Tsinghua University, [2]Shanghai Jiao Tong University, [3]Zhejiang University
{zhangjc21, sym21, wwg18, j-zhang19, nx20}@mails.tsinghua.edu.cn, Jinm@sjtu.edu.cn, guoxz@zju.edu.cn, heyuan@tsinghua.edu.cn

ABSTRACT

This paper presents RFinder, a handheld RFID localization system that can accurately localize an in-concrete RFID tag. Such a system facilitates RFID applications in construction quality control. However, the challenge we meet in designing such a system is to achieve accurate RFID localization in a compact (*e.g.*, with only one antenna) and mobile form.

To solve this problem, we opportunistically combine the sensing ability of the RFID and the Inertial Measurement Unit (IMU) sensor that is widely embedded in most handheld RFID readers. Specifically, the user just needs to hold the handheld device and move it in the air. The movement of the device causes changes in 1) RFID measurement phase, and 2) motion sensor data (*e.g.*, acceleration) captured by IMU. We find that if the tag's direction relative to the tag is almost not changed, it is possible to establish a correlation between the velocity calculated from acceleration and that of the RFID phase, thereby enabling us to localize the tag's AoA without the precise position of the antenna. We build a signal preprocessing and matching workflow to better fuse the two kinds of data. Experiments show that RFinder can achieve an 11° 3D AoA estimation accuracy at the range of 2.5m.

CCS CONCEPTS

• **Information systems** → **Location based services**;

KEYWORDS

RFID, Localization, Prefabricated Buildings

1 INTRODUCTION

Construction quality control is one of the most critical aspects of any construction project. Poorly constructed buildings not only incur wasted time, resources, and materials for re-construction but also lead to life-threatening accidents, such as the collapse of buildings and bridges. It is reported that in 2021, the collapse of the structure caused 1630 deaths in India [1]. One major reason behind these accidents is the use of unqualified building materials. So we need an effective and efficient method to achieve life-cycle management for integrity and safety construction.

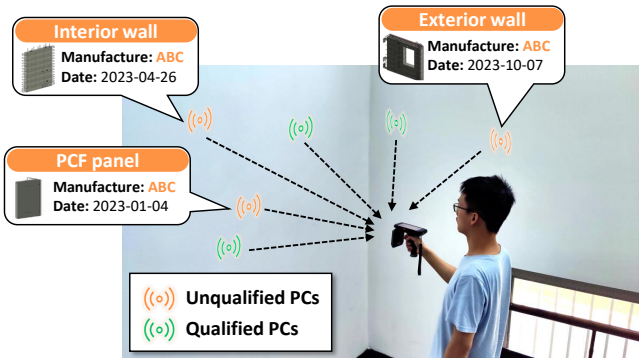

Figure 1: The application scenario of RFinder.

In recent years, Radio Frequency Identification (RFID) technology [21] is evolving as a major technology enabler for building quality control [5]. Several companies, such as RFIDHY [29] and SEIKO [27] have proposed RFID tags that can be mounted on metal and embedded in concrete to monitor the structural health of the building. Compared with other identification technologies such as QR code and AirTag [4], RFID provides the advantage of non-line-of-sight and battery-free communication, thus is more suitable for building quality control – by embedding RFID tags into the prefabricated components (PCs)[1], we can perform an all-process retrieving of each PC's information, such as its manufacturing date and quality standards, no matter the PCs are stacked in the warehouse, shipped on board, or already installed in the building. Fig. 1 shows an example of RFID-based building quality management. In this case, PCs released by a certain manufacturer are found to be potentially unqualified after the building is completed. In such an RFID-based building

*Yuan He is the corresponding author.

[1]Prefabricated components refer to pre-engineered elements of a building (such as walls, roofs, floors) that are manufactured off-site to enhance construction efficiency and minimize disruptions on-site.

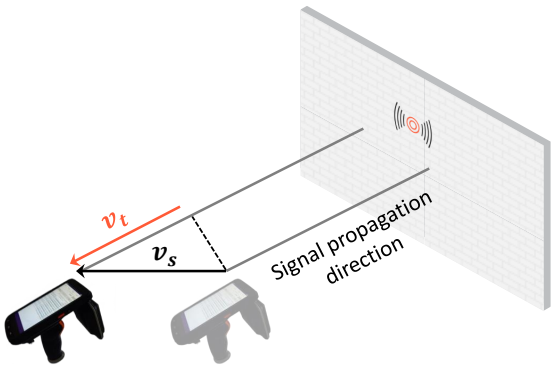

Figure 2: An illustration of RFinder's key idea.

quality management system, RFID localization technique is leveraged to build a mapping between the prefabricated components we see in the physical world to the RFID signal we have received. Specifically, when querying a tag embedded in a specific component, all the tags around can response their information, making it difficult to identify which one is from the specified component. So, we need an RFID localization to map the tags with their exact locations. This technology has significant applications in Building Information Modeling (BIM[7]). For instance, to accurately model a building, the positions of the components must be input into the model to facilitate lifecycle maintenance of the building[30].

However, realizing the above vision requires an RFID localization system to satisfy the following three requirements:

1) **Portable.** Since the target PCs can be distributed across different floors and rooms in a building, the worker has to walk around the building to query and localize the tags embedded in the wall. So the proposed localization method should be *compact*, *portable*, and can work even in mobility scenarios.
2) **In-concrete localization.** In construction control scenarios, tags are usually embedded inside the prefabricated components, which are made of reinforced concrete. Since the concrete can largely attenuate and distort the signal propagating through it, we need a robust localization method that can work with a weak signal and non-ideal signal metrics.
3) **High accuracy.** Since tags are densely deployed inside the wall (*e.g.*, with a decimeter-level, the dimension of components is shown in Tab. 1), the localization method should be accurate enough so that different tags can be spatially distinguished.

Unfortunately, no system exists today that can realize all three goals simultaneously. Accurate RFID localization typically requires bulky antenna arrays or multiple antennas [6, 22, 36–38], which are clearly unavailable on portable devices. To avoid bulky infrastructures, researchers have considered mounting antennas on mobile robots to emulate antenna arrays (*i.e.*, SAR) [3, 23, 31, 32]. However, these methods require moving the robot and/or tag on well-defined trajectories, making them ill-suited for handheld human mobility. To address the above problems, some recent works, like POLAR [15] and X-AR [8], propose portable or wearable localization systems by combining the RFID signal and the vision signal. Specifically, these systems use a camera to perform self-tracking and then combine the RFID signal obtained at different locations or along a known trajectory to perform accurate localization. However, these systems suffer the following two problems. First, POLAR localizes the target leveraging ToF (time-of-flight) of the RFID signal. However, the speed of the signal changes when it propagates through the concrete wall, which undermines the ToF and thus leads to serious localization error. Second, they both use visual-inertial odometry (VIO) technique to perform self-tracking. However, VIO technique is sensitive to sudden illumination changes, fast motions of the user, and other moving objects in the environment, which are common and inevitable on construction sites. In Tab. 2 we make a comparison with the state-of-the-art works. Comparing to other works, RFinder can be implemented on handheld devices and is also compatible with commercial devices. Additionally, it can adapt to existing RFID reading protocols and dynamic environments.

Table 1: Dimensions of common prefabricated components.

prefabricated components	thickness (mm)	width (mm)	height (mm)
external wall panels	100-300	600-3000	2400-3600
internal wall panels	100-200	600-3000	2400-3600
composite floor slabs	120-200	600-2400	3000-12000
solid prefabricated floor slabs	150-250	600-2000	3000-12000
prefabricated columns	300-1000	300-1000	3000-6000
prefabricated beams	200-600	300-1500	3000-18000
L-shaped retaining walls	150-300	1000-4000	1000-6000
prefabricated window sills	/	200-500	1000-3000
prefabricated balcony slabs	150-300	1000-2500	2000-5000

To distinguish the position of different components, we reviewed relevant standards from Precast/Prestressed Concrete Institute (PCI)[26] and National Precast Concrete Association (NPCA)[24]. We learn about some commonly used typical dimensions of prefabricated components (Tab. 1). These components generally have thicknesses ranging from 100 to 300mm, and widths typically ranging from 500mm to several meters. Some components, such as beams and columns, have narrower widths. However, these components are typically spaced further apart, making them easier to distinguish compared to panels and slabs. To achieve effective differentiation, our average localization accuracy must be within 500mm. However, simple methods, such as the RSSI-based approach mentioned in Tab. 1, with an average localization accuracy

Table 2: Comparisons of related works on RFID localization.

Reference	Localization Target	Accuracy	Data	Devices	Antenna number	Frequency bandwidth	Portablity
Tagoram[41]	Moving luggage	< 1cm	Phase,RSSI	Commercial Devices	> 2	Multiple frequencies	Fixed
3D-omnitrack[20]	Moving tag	≈ 10cm	Phase,RSSI	Commercial Devices	3	Multiple frequencies	Fixed
Tag-Focus[43]	Moving tag	< 1cm	Phase,Image	Commercial Reader + Camera	1	Single frequency	Fixed
Meta-Sight[40]	Static tags	< 20cm	Phase	Customized Antenna	Meta-surface Antenna	Single frequency	Fixed
POLAR[15]	Static tags	≈ 10cm	Phase,Image	Customized Antenna and Readers	4	Multiple frequencies	Handheld, Mobile
X-AR[8]	Static tags	≈ 10cm	Phase,Image	Customized Antenna and Commercial Reader	1	Multiple frequencies	Wearable, Mobile
RTLS[9]	Static tags	≈ 2m	RSSI	Commercial Devices	4	Single frequency	Fixed
Xiao, *et al.*[39]	Static tags	≈ 1m	RSSI	Commercial Devices	4	Single frequency	Fixed
RFinder	**Embedded static tags**	35cm	**Phase,Acceleration**	**Commercial Devices**	**1**	**Single frequency**	**Handheld, Mobile**

of over 1m, are inadequate for distinguishing the positions of the components.

We in this paper present RFinder, an RFID localization technique that achieves accurate and in-concrete RFID localization in mobility and portable form, using only one antenna. We achieve this by opportunistically combining the sensing ability of the RFID and the IMU sensor that is widely embedded in most handheld RFID readers. We find that when the user moves, both the inertial data collected by the IMU sensor and the phase variation collected by the reader can reflect user's mobility pattern. As shown in Fig. 2, the IMU captures the user's movement velocity (denoted as v_s), while the phase variation captures the rate of change in reader-to-tag distance (termed as radial velocity, denoted as v_t). The angle between v_s and v_t is the AoA of the tag's signal. By moving the reader along different directions in the 3D space, we can obtain the 3D AoA of the tag's signal (*i.e.*, the polar angle and the azimuthal angle). Then, if we can measure the antenna-to-wall distance (details can be found in Sec. 4.1), we can obtain the exact location of the tag on the 3D spherical coordinate centered at the user.

Note that RFinder is naturally resistant to the impact of the concrete wall due to the fact that: i) it uses narrowband signal for localization, thus avoiding the frequency selective attenuation brought by the concrete wall and reducing the chances of being interfered with; and ii) it estimates tag's AoA by observing the *change* in phase measurement during the antenna's movement, thus the additional phase rotation and signal loss caused by the concrete wall can be removed by performing differential on the received signal.

However, the main challenge is that IMU and RFID signals are sampled at different rates and devices (*i.e.*, IMU at 100-200Hz and RFID at 50Hz). More seriously, RFID's sampling process is unstable and suffers occasional data loss due to the random channel access protocol [10] used by RFID and the inevitable variation in wireless channels. So we need a method to match the two signals in both the time domain and measurement coordinate.

We address this problem with an advanced data-matching method base on DTW algorithm. The proposed method can automatically stretch and scale the data series and finally find an optimal alignment between them.

Contribution. We make the following contributions:

- We present RFinder, the first to demonstrate a portable RFID localization system that can accurately localize a tag inside the concrete wall, using a COTS RFID reader with only one antenna. RFinder facilitates more effective and efficient construction quality control.
- We explore the relationship between IMU data and phase measurement, and based on this we propose an accurate AoA estimation method. The method is then embedded into a complete system that overcomes practical challenges, including the drifting in the IMU sensor and the misalignment between IMU data and phase measurement.
- We evaluate the performance of RFinder by conducting comprehensive experiments under various settings. Results show that the RFinder can provide AoA estimation accuracy within 11° and location error within 0.35 m within the range of 2.5m.

2 UNDERSTANDING THE SIGNAL PHASE IN THE CONCRETE STRUCTURE

We start with an analysis of how RFID signals behave as they propagate inside a concrete wall, and why RFinder is resistant to the in-concrete propagation of the RFID signal.

At first, we will introduce the main factors that influence the propagation characteristics of electromagnetic waves within non-conductive materials: dielectric permittivity ϵ_r. The concrete's ϵ_r is a variable value that is highly related to both the signal frequency (which determines the imaginary part of ϵ_r) and the features of the concrete. Typically, the relative dielectric permittivity ϵ_r of concrete falls within the range from 6 to 12 [13].

When EM waves enter the concrete, their propagation speed changes due to the change in the dielectric permittivity of the propagation medium. Specifically, their speed in concrete is given by $v = \frac{c}{\sqrt{\epsilon_r}}$, where c is the speed of light in vacuum and air. Since the frequency f of the incident wave remains constant in different materials, the wavelength λ of the signal changes with the propagation speed as $\lambda = \frac{v}{f}$.

Besides the propagation speed, the concrete also changes the signal's propagation direction. This phenomenon follows

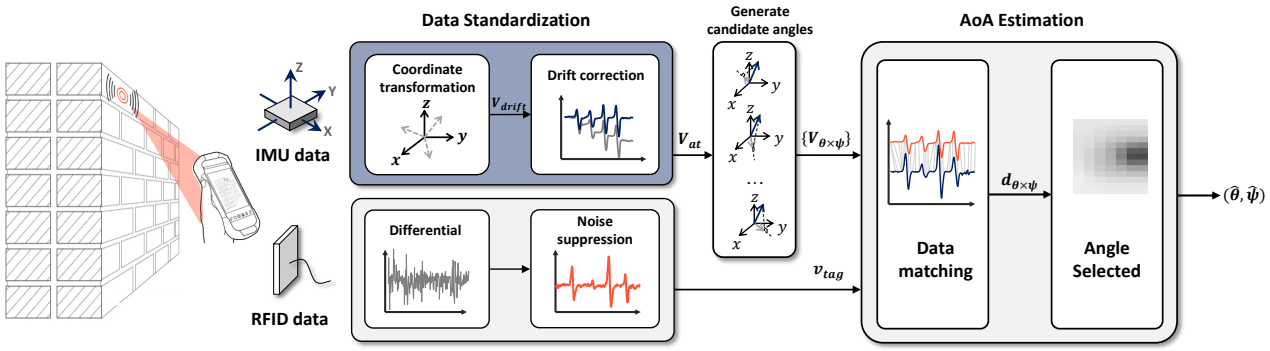

Figure 3: System overview.

the law of refraction as:

$$\frac{\sin\theta_1}{\sin\theta_2} = \frac{\sqrt{\epsilon_{r2}}}{\sqrt{\epsilon_{r1}}} \tag{1}$$

where θ_1 and θ_2 are incident and refraction angles, respectively.

Fig. 4 illustrates how the signal travels inside the concrete. We assume that the depth of the RFID tag inside the concrete is d, then the propagation distance of the signal (denoted as l) can be represented as:

$$l = \frac{d}{tan(\theta_2)} \tag{2}$$

By combining Eqs. (1) and (2), we can calculate the change in phase caused by the concrete as:

$$\Delta\phi = \frac{4\pi l}{\lambda_{con}} = \frac{4\pi l\sqrt{\epsilon_r}}{\lambda_{air}} \tag{3}$$

where λ_{con} and λ_{air} are the wavelength in the concrete and the air, respectively. As can be seen, given a certain dielectric permittivity ϵ_r, the change in signal phase is highly related to the incident angle θ_2 and the depth of the tag d.

Fig. 5 shows the phase changes under different incident angle θ_1 and tag depth d. The results are obtained by setting $\epsilon_r = 6$, which is the minimum dielectric permittivity that concrete can achieve. As expected, the change in the phase increases significantly with the incident angle and the depth of the tag. When the tag depth reaches 15cm, the concrete brings a more than 0.2 rad phase change between incident angle 0° and 80°, which inevitably leads to serious localization errors. This is also why some of the existing portable localization methods cannot perform in-concrete RFID localization.

Fortunately, however, the phase rotation caused by the concrete wall does not affect the localization performance of RFinder. This is because that RFinder estimates the AoA of the tag by observing the *change* in phase, rather than the absolute value. So, the impact of concrete wall can be easily removed by performing differential on the phase signal, if the phase rotation brought by the wall remains stable during the movement of the reader antenna. This assumption holds in our scenario. Specifically, consider a case where the user stands 2m away from the wall, and moves the reader antenna with a moving distance of 30cm. In this case, the change in incident angle during the movement is less than 10°. If the tag's depth is 3cm, a 10° change in incident angle results in only 0.01 rad change in phase, according to Fig. 5, which is neglectable in our method.

3 OVERVIEW

RFinder is a system that can accurately localize RFID-tagged items with a handheld device. It achieves fine-grained 3D localization with only one antenna. RFinder consists of an IMU sensor and a COTS (commercial off-the-shelf) RFID reader. To localize a target, the user only needs to hold the antenna and move it in the air, during which the reader queries the tags with a 920.625MHz query signal and collects the phase variation of the tag's signal; the IMU sensor measures the 6-DoF inertial data of the user's motion. RFinder then estimates the AoA of the tag by comparing the two sources of data. The tag's location can be further estimated by measuring the antenna-to-wall distance or combining AoAs measured on multiple locations.

Fig. 3 shows the system architecture of RFinder, which is composed of two modules:

Data standardization. This module pre-processes the phase and IMU data for further fusion. It consists of two parts: i) *differential noise suppression module*, which mitigates the high-frequency noises introduced by signal differential; ii) *IMU drift correction module*, which aims to estimate and calibrate the drift error of the IMU data.

AoA estimation. This module aims to estimate the AoA of the tag's signal by comparing the IMU data and the phase measurements. It consists of two parts: i) *data matching module*, which synchronizes and aligns the IMU data and phase data (two series of data collected with different sampling

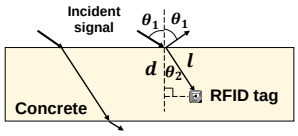

Figure 4: Signal propagation in the concrete.

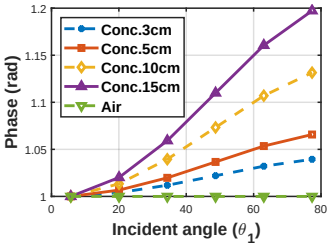

Figure 5: Phase distortion.

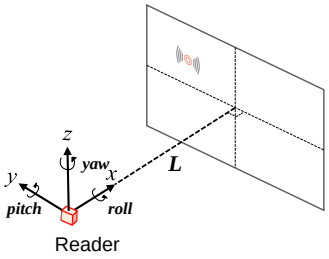

Figure 6: 3D localization.

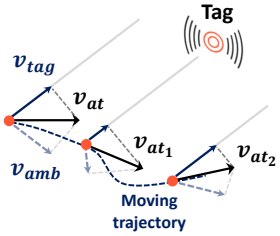

Figure 7: Basic model.

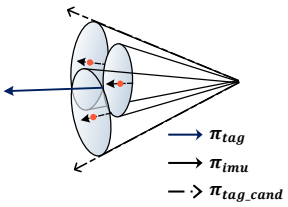

Figure 8: 3D AoA estimation.

rates) with an enhanced DTW algorithm; and ii) *angle selection module*, which compares the IMU data and the phase data to estimate the most likely AoA of the tag's signal.

4 DESIGN

In this section, we introduce the core design of RFinder, where we first introduce the basic model used for AoA estimation, and then illustrate the system design in detail.

4.1 Localization Model

Data matching based AoA. RFinder aims to address the crucial limitation inherent in traditional AoA approaches, namely, the dependence on the accurate location attributes of the antenna. Unlike conventional methods, our approach offers an AoA estimation model that circumvents the requirement for the accurate locations of the antennas, thus providing a more flexible and efficient solution for fine-grained RFID localization.

The basic idea of RFinder is to estimate the tag's AoA by comparing the velocity value measured by IMU and the reader. Specifically, when the user moves, we can obtain the user's moving velocity (denoted as V_{at}) by taking the integral of the acceleration value measured by IMU. We can also obtain the rate of change in antenna-to-tag distance (denoted as V_{tag}) by observing the tag's phase differential caused by the user's movement. The relation between the two velocity measurement is illustrated in Fig. 7. As can be seen, V_{tag} is always equal to the projection of V_{at} in tag's direction. So we have:

$$V_{tag} = \cos(\theta) \cdot V_{at} \tag{4}$$

Based on the above equation, we can figure out the direction of the tag (θ). However, given the measured $\|V_{tag}\|$ and V_{at}, we can find two candidate angles that satisfy the above equation because $\cos(\theta) = \cos(-\theta)$. Fig. 7 shows that V_{amb} have the same length as V_{tag}, which is the ambiguous vector. To distinguish the real direction and the ambiguous direction, we move the antenna with a varying velocity in the plane (See in Fig. 7). Since the ambiguous direction changes with different velocities while the real direction are coincide across different velocities, we can eliminate that ambiguity by combining the result obtained on different velocities.

This method can be easily extended to the 3D space, where the ambiguous directions for a certain pair of V_{tag} and V_{at} form a conical surface, as shown in Fig. 8. Similar to the 2D case, we can change the reader's moving direction and velocity to obtain many cones. The intersection between more than three cones can give the real direction of the tag $\boldsymbol{\pi}_{tag}$, as shown in Fig. 8.

Angle search and 3D-localization. More specifically, tag's direction can be estimated by finding the direction $\boldsymbol{\pi}_{tag}$ that optimizes the following equation:

$$\boldsymbol{\pi}_{tag}(\theta^*, \psi^*) \leftarrow \arg\min_{\theta,\psi} \left[\sum_{j}^{N} \left(\frac{\boldsymbol{V}_{at,j} \cdot \boldsymbol{\pi}_{\theta,\psi}}{\|\boldsymbol{\pi}_{\theta,\psi}\|} - \|\boldsymbol{V}_{tag,j}\| \right)^2 \right] \tag{5}$$

Here $\boldsymbol{\pi}_{tag}(\theta^*, \psi^*)$ denotes the AoA of the tag with respect to the reader (where θ and ψ are pitch angle and yaw angle). $\boldsymbol{\pi}_{\theta,\psi}$ is the unit vector in the (θ, ψ) direction. $\boldsymbol{V}_{at,j}$ and $\boldsymbol{V}_{tag,j}$ are IMU velocity and the velocity with respect to tag at time j, respectively. In practice, the reader's antenna typically covers only the space in front of it. So in the searching process, we only need to traverse half of the entire space by setting $\theta, \psi \in [-\frac{\pi}{2}, \frac{\pi}{2}]$.

Now we have obtained the 3D AoA of the tag, *i.e.*, $\boldsymbol{\pi}_{tag}(\theta^*, \psi^*)$. Then, as shown in Fig. 6, we can estimate the tag's 3D location $LOC_{tag}(x, y, z)$ as:

$$
\begin{aligned}
LOC_{tag}(x,y,z) &= \boldsymbol{\pi}_{tag}(x=L) \\
&= [cos\psi^* cos\theta^*, -sin\theta^*, \\
&\quad sin\psi^* cos\theta^*] \frac{L}{cos\psi^* cos\theta^*}
\end{aligned} \tag{6}
$$

where L is the vertical distance between reader and the wall, as shown in Fig. 6. It can be measured by adding a proximity sensor to the handheld RFID reader or letting the user stand in a marked position with a known distance to the wall.

4.2 Data Standardization

While the model proposed in Sec. 4.1 is straightforward, embedding it into a practical system needs to solve several challenges, such as phase noise, IMU drift error, and the difference in the sampling rates of the RFID reader and the IMU sensor, all of which can significantly impact the system's performance. In this subsection, we will detail the methodology to address these problems.

Phase noise suppression. The phase reading θ of an RFID tag contains four parts:

$$
\theta = (\theta_{prop} + \theta_{orient} + \theta_{tag} + \theta_{antenna}) \ mod \ 2\pi \tag{7}
$$

where $\theta_{prop} = 2\pi \times \frac{2d}{\lambda}$ is the phase change caused by the signal's round-trip propagation along the antenna-tag distance d and λ refers to the wavelength of the signal. θ_{tag} and $\theta_{antenna}$ are constant values that are caused by the imperfect hardware of the tag and antenna, respectively. θ_{orient} is also considered invariant in our system if the user does not rotate the antenna during the movement.

We can retrieve the change rate of the antenna-tag distance and cancel out the other invariant part of the phase by taking the first derivative of the unwrapped phase values:

$$
\|\boldsymbol{V}_{tag}\| = \frac{\lambda}{4\pi} \frac{\Delta\theta}{\Delta t} \tag{8}
$$

Unfortunately, the differentiation operation may amplify the inherent high-frequency noise contained in the phase measurement, which further leads to a large error in velocity estimation. We solve this problem based on the fact that the frequency of human movement is generally between 0-5Hz while the noise signal is mainly distributed in the high-frequency band. Fig. 9 shows the PSD (Power Spectral Density) of the phase and the velocity value derived from the phase measurements, which proves our assumption above. So, we can easily remove the high-frequency noise using the low-pass Butterworth filter.

IMU drift correction. Another challenge in IMU-based velocity estimation is the serious drift error in the gyroscopes and accelerometers, which accumulates when acceleration integration is performed. To understand the impact of IMU acceleration integration error, we place the IMU on a reciprocating machine and estimate the moving velocity of the IMU by integrating the acceleration value reported by the IMU. Fig. 11 shows how the velocity error accumulates with time. We make two key observations: i) the velocity error accumulates to nearly 10m/s within 22 seconds; and ii) although the reciprocator moves with a constant speed, the velocity value is non-linear in a relatively long time span.

The above observation tells that, on one hand, we cannot estimate and compensate the velocity error by performing linear fitting or low pass filter to the entire velocity sequence. On the other hand, it is hard to build a non-linear error model due to the inherent variability in noise levels among different IMUs.

We solve this problem based on the observation that, in a short period of time, the velocity error changes linearly with time. So, instead of performing continuous movement, we guide the user to perform intermittent movement with the antenna, so that the velocity error accumulated in each motion segment can be considered as changing linearly with time. RFinder can then estimate and compensate the velocity error in each motion segment through linear fitting Fig. 12.

4.3 Data Matching

In the basic model introduced in Sec. 4.1, we assume that the RFID signal and IMU signal are completely aligned in the time domain. This assumption is however unrealistic in practice due to the difference in the sampling rate of the RFID reader and the IMU sensor (30Hz≤RFID≤60Hz, IMU≈100Hz). To provide a more detailed illustration of the issue, we perform an experiment to collect real reading traces of IMU sensor and RFID reader, and shown in Fig. 10 the distribution of the sampling interval of the two devices. The results tell that: i) the sampling interval of the two devices are quite different; ii) the sampling rate of both the two devices show high instability. So, the two streams $\{V_{at_1}, V_{at_2}, ...\}$ and $\{V_{tag_1}, V_{tag_2}, ...\}$ are misaligned with each other.

To match the two series, a straightforward method is to perform interpolation. However, it is challenging to align the two series because they are collected by two different devices which are not tightly synchronized. More seriously, the timestamps of the data record only the time when the data arrive at the the laptop, rather than the time when the data is physically sampled by the reader or the IMU sensor. The unstable and random data processing delay makes it more difficult to synchronize the two series.

DTW background. We solve the above problem with Dynamic Time Warping (DTW), a typical signal-matching technique that is designed to match two temporal sequences that do not sync up perfectly. Given two time series ($\mathbf{S^a} = \{S_1^a, ..., S_M^a\}$ and $\mathbf{S^b} = \{S_1^b, ..., S_N^b\}$), and a cost metric D, DTW finds an alignment that maps each point in the first series to

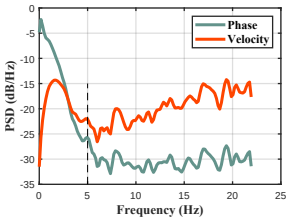

Figure 9: Differential noise suppression.

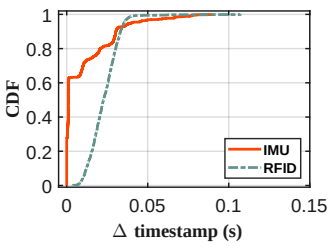

Figure 10: Time difference.

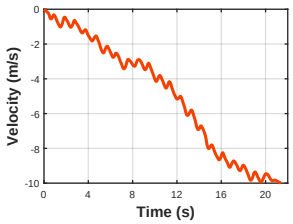

Figure 11: IMU non-linear drift.

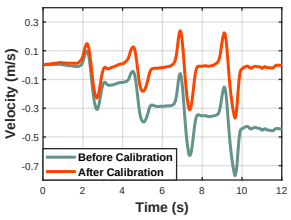

Figure 12: Separated calibration.

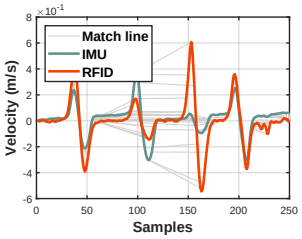

(a) DTW matching result.

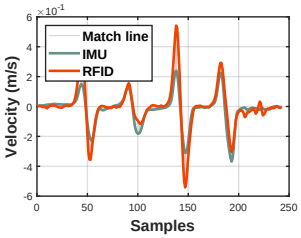

(b) TDTW matching result.

Figure 13: TDTW performance.

one or more points in the second series, such that the cost of the mapping summed over all point pairs is minimized.

Typically, the cost of mapping two points S_i^a and S_j^a is given by

$$d(i,j) = (S_i^a - S_j^b)^2 \tag{9}$$

Given this input, DTW searches for the best alignment of the two series that minimizes the global cost, using standard dynamic programming. Here, the optimal global cost of DTW can be recursively calculated by:

$$D_{DTW}(V_a^i, V_b^j) = d(i,j) + \min \begin{cases} D_{DTW}(V_a^{i-1}, V_b^{j-1}) \\ D_{DTW}(V_a^{i-1}, V_b^j) \\ D_{DTW}(V_a^i, V_b^{j-1}) \end{cases} \tag{10}$$

where $D_{DTW}(V_a^i, V_b^j)$ is the minimum sum cost at position (i, j).

Time-weighted DTW. Despite its wide use, DTW cannot be directly applied in our scenario because it suffers serious error in matching two series that are scaled quite differently across clips. Specifically, in aligning two series, DTW considers only the distance (*i.e.*, mapping cost) between point pairs, while ignores their time offsets. As a result, two matching points may have a big gap in time domain. Fig. 13 (a) shows how DTW algorithm matches the velocity series calculated obtained by IMU sensor and RFID reader. As can be seen, to minimize the distance summed over all point pairs, DTW matches the IMU signals sampled in the second moving period to the RFID signals sampled in the third moving period.

To address this problem, we propose a novel series matching method named TDTW (Time-weighted DTW), which considers both the velocity difference and the time offset between to points in calculating the mapping cost:

$$D(V_a^i, V_b^j) = \left| \frac{i-j}{M} \right|^2 + d(i,j) + \min \begin{cases} D(V_a^{i-1}, V_b^{j-1}) \\ D(V_a^{i-1}, V_b^j) \\ D(V_a^i, V_b^{j-1}) \end{cases} \tag{11}$$

where $|\frac{i-j}{M}|^2$ is the norm square distance between two points on the timeline.

Fig. 13 (b) shows the matching result achieved by the proposed TDTW algorithm. As can be seen, TDTW is capable of finding the best matching between the two series, despiting the difference in amplitude scaling and local time shifting of RFID and IMU signals.

5 EVALUATION

5.1 Implementation and Methodology

Implementation. We implement RFinder using the Impinj R420 RFID reader [2], which is connected with a Laird S9025PR antenna [35], The reader works at a single frequency of 920.625MHz and the gain of the antenna is set at 8.5dBi. According to FCC regulations [19], for the transmitter that works at a signal bandwidth that is less than 250kHz without frequency hopping. The RFID system samples the tag's signal at a reading rate ranging from 30~50Hz. To measure the moving velocity of the Reader, we further attach an N200 IMU sensor (supplied by WHEELTEC [16]) on the antenna, as shown in Fig. 14. The IMU sensor samples the 6-DoF movement of the reader with a frequency of 100Hz. It should be noted that there are extensive commodity handheld RFID systems [28] that operate with Android and iOS mobile phones, which are usually equipped with a low-cost IMU. Our system can be easily deployed on these devices and we leave it in our future work.

Methodology. In the experiments, we embed the RFID tags into $30cm \times 30cm \times 15cm$ concrete components with a depth of 3cm, as shown in Fig. 14. We use standard C30 concrete [14] which consists of three layers, where the upper two layers are made of poured cement and the third layer is composed of stones and steel bar meshes. We put the components

on a metallic shelf (as shown in Fig. 14) and observe how the performance of RFinder is affected by the following factors:

i) The relative positions between the component and the reader antenna, which is further determined by three different parameters: the deployment height H; the reader-to-shelf distance L; and the horizontal offset W, as shown in Fig. 14. We tested 81 different relative positions and the results are shown in Sec. 5.2.

ii) User's operation modes, such as moving the device at different distances in the air and different speeds.

iii) Concrete related factors, such as the composition of the concrete and the buried depth of the tag.

Benchmark. We conduct a benchmark experiment to compare the signal attenuation when the tag is embedded in the concrete and air. In the experiment, we first place the tag at a height of H = 0.75m and fix the height of antenna at 0.75m. We vary the antenna-to-shelf distance L from 0.5m to 2m with a step of 0.5m and vary the horizontal offset of the antenna from -1.0m to 1.0m, with a step of 0.2m. We read the tag's RSSI on each of the 44 positions. As a comparison, we further repeat the above experiment by embedding the tag in a prefabricated component and place the component at a height of 0.75m. The results obtained in air and in concrete are shown in Fig. 15.

As can be seen, in both the scenarios there are areas where the signal cannot be received, known as signal blind spots. While, compared with the case in the air, signal propagating in the concrete suffers an additional 10dB attenuation. Another important observation is that we can find more blind spot in the in-concrete cases. This may bring difficulties to the antenna array based or SAR (Synthetic Aperture Radar) based localization methods, which need to combine the signal that received at different locations for accurate RFID localization. While, different from those methods, RFinder can accurately localize a tag based on the signal collected in one spot (with micro-mobility within a distance of few decimetres). That is to say, it can achieve accurate localization as long as it can find a "sighted" spot in front of the wall, which makes it highly highly resistant to the impact of the concrete wall.

5.2 Overall Performance

In this section, we evaluate the overall performance of RFinder under different relative position between the tag and the user. In the experiment, we place the concrete component at three different heights: H=0.25m, 0.75m, and 1.25m, where the H refers to the height of the tag which is embedded in the concrete. The reader antenna's height is fixed at H = 1.0m, and the distance between the antenna and the wall (L) varies from 1m to 2m with a step of 0.5m. The horizontal offset of the antenna (W) ranges from -0.8m to 0.8m, with a step of 0.2m.

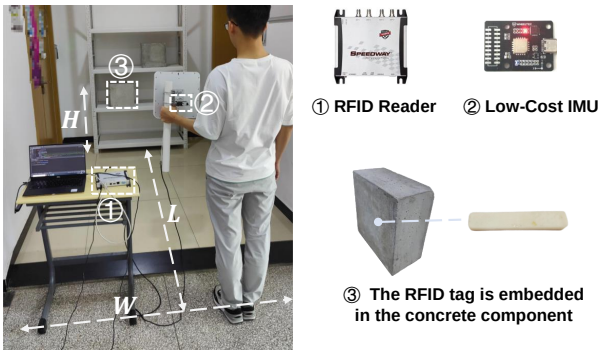

Figure 14: System deployment.

Fig. 16 shows the results under different positions. Among all 69 points (excluding blind spots), RFinder achieves a 11.3° mean error, with a variance of 2.7°.

Fig. 16 further shows the AoA error obtained under different antenna-to-wall distance L. One counterintuitive observation in this figure is that the accuracy obtained at shorter L is not always better than that obtained at longer L. This can be attributed to the field of view (FoV) angle of the antenna. Due to the presence of the FoV, a shorter antenna-to-wall distance may lead to a larger tag-to-antenna orientation, leading to a lower probability that the tag can be radiated by the reader. Additionally, in our model, we assume that the distance between the tag and the antenna is much larger than the movement distance of the antenna. However, when the antenna locates closer to the tag, there is a larger variation of the tag-to-reader AoA when the user moves the antenna, resulting in greater error in AoA estimation.

We further evaluate RFinder's localization accuracy. Specifically, based on the AoA estimation and the antenna-to-wall distance L, we estimate the exact location of the tag. Fig. 17 (b) shows the results obtained under different L. The median location error is 0.2m, 0.36m and 0.40m, when we set L at 1m, 1.5m and 2m, respectively. Correspondingly, the 95^{th} location error is 0.39m, 0.60m and 0.78m, respectively.

5.3 Impact factors

One important factor that can affect the RFinder's performance is the user's motion pattern, such as moving distance, and speed. In this section, We evaluate how these factors affect the performance of RFinder. Besides the motion pattern, we in this section also evaluate RFinder's performance under different concrete structures and the buried depth of the tag. In all the experiments in this section, the tag is placed at $[H, W, L]$ = $[1m, 0m, 1.5m]$, and the user stands at $[H, W, L]$ = $[1m, 0m, 0m]$ on the coordination shown in Fig. 14.

Movement speed. We first evaluate RFinder's performance at two different speeds. In the experiment, we move the antenna in four different directions. In each direction, we

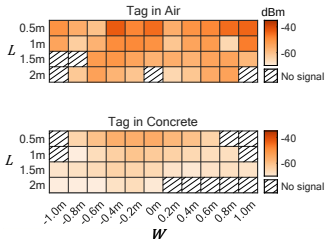

Figure 15: RSSI measurement.

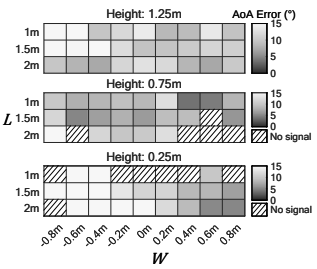

Figure 16: Mean AoA error.

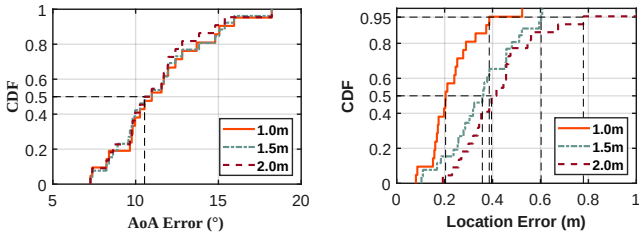

(a) AoA error.

(b) Location error.

Figure 17: Overall performance in different L.

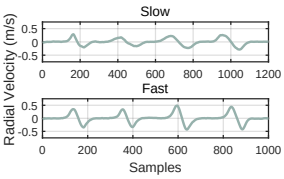

(a) Different moving speeds.

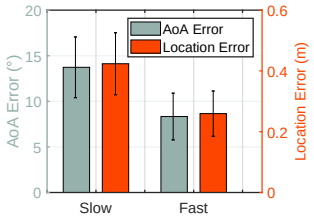

(b) AoA and location error.

Figure 18: Impact of the moving speed.

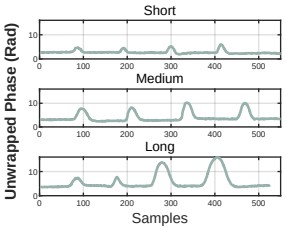

(a) Different moving distance.

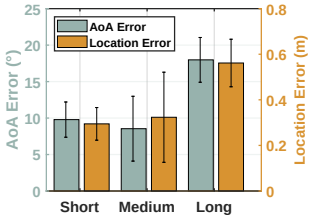

(b) AoA and location error.

Figure 19: Impact of the moving distance.

perform round-trip movement with two different speeds, *i.e.*, slow (about $0.25m/s$) and fast (about $0.5m/s$). The corresponding radial velocity measured under the two moving speeds is shown in Fig. 18 (a). Note that we categorize them into two types of velocities by the average velocity of the four movements. Fig. 18 (b) shows the AoA error and location error obtained under different moving speeds. The results show that RFinder achieves a better AoA estimation accuracy (*i.e.*, 8.3° on average) when the user moves the antenna at a fast speed. The accuracy decreases to 13.7° when the antenna moves at a slow speed. This is because the IMU and phase signals achieve a higher SNR at a higher moving speed.

Movement distance. In this experiment, we move the antenna at a fast speed, while changing the movement distance from 0.1m (short), 0.2m, to 0.3m, with a step of 0.1m. The phase measurements obtained under different movement distances are shown in Fig. 19 (a). As can be seen, the phase change measured under the shortest moving distance is about 2.5 rad. Fig. 19 (b) shows the AoA accuracy obtained under different movement distances. As can be seen, RFinder achieves the best performance when the movement distance is 0.2m. When the movement distance increases to 0.3m, the AoA estimation error increases to 18°. This is because when the antenna moves with a longer distance, the AoA of the tag's signal will change during the movement, which violates the assumption underlying our signal model in Sec. 4.1, and thus brings higher AoA estimation error.

Different concrete structure. In most concrete components, steel bars are used to enhance their tensile strength. In our experiment, we embed a steel reinforcement mesh at the bottom of the concrete with dimensions of $30cm \times 30cm$. Then we place stones on the mesh. The tag is embedded at the upper part of the concrete with a depth of $3cm$. Another concrete component is totally made of concrete, which consists of cement, sand, and stone. We place the component at $[H, W, L] = [1m, 0m, 1.5m]$ and the location of user is at $[H, L] = [1m, 1.5m]$ while the W varies from $-0.8m$ to $0.8m$ with $20cm$ gap. Fig. 20 shows that the median location errors of the two types of components are $0.21m$ and $0.24m$ and the corresponding median AoA errors are both 7.8°, with a very small difference observed in the results. This is because the reflected signal from the tag reaches the steel mesh and undergoes a thick layer of concrete before reaching the receiver. The multipath effects of this part are very weak and can not affect the directly reflected signal of the tag.

Different burial depths of the tag. In our study, we evaluate the impact of different burial depths of the tag in the concrete. We placed the tag at two different depths: $3cm$ depth and $6cm$ depth. By comparing the localization performance at these different depths, we aimed to assess the influence of burial depth on the system's performance. Under the condition of a burial depth of 6cm, we are only able to read the tag within a small region of $L = 1m$. Therefore, in all our experiments, We place the component at $[H, W, L] = [1m, 0m, 1m]$ and the location of the user is at $[H, L] = [1m, 1m]$ while the W varies from $-0.6m$ to $0.4m$ with $20cm$ gap. Fig. 21 shows that the median location errors of $3cm$ and $6cm$ depth are $0.13m$ and $0.24m$, respectively. Besides, the corresponding median AoA errors are 7.46° and 8.34°, respectively. This

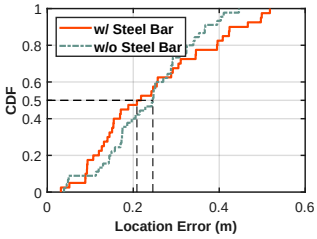

Figure 20: Impact of the steel bar in the concrete.

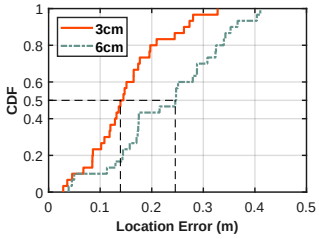

Figure 21: Impact of the burial depths of RFID tag.

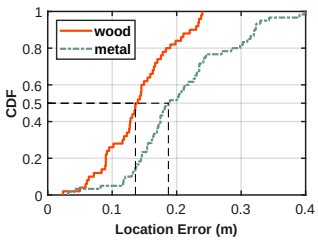

Figure 22: Impact of the different environments.

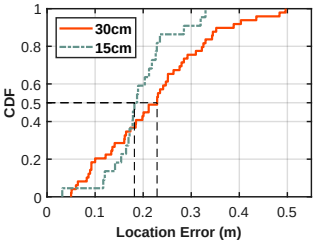

Figure 23: Impact of the thickness of components.

indicates that the depth where the tag is buried has a significant impact on the strength of the reflected signal. However, its impact on RFinder is limited.

Different materials of the holding shelf. In the system setup described above, a metal shelf is used to support the concrete components. To investigate the impact of different materials, we replaced the metal shelf with a wooden one and repeated the experiments in two different environments. The results in Fig. 22 demonstrate that using a wooden shelf results in a lower location error compared to the metal one. However, in real-world building construction, metal components (*e.g.,* steel bars) are commonly used to support concrete structures. Consequently, the performance of RFinder in practical applications is more aligned with the results obtained using the metal shelf. In our future work, we will try to mitigate the impact of metal components.

Different thickness of components. In reality, prefabricated components can vary in thickness. Here, thickness refers to the dimension of the component perpendicular to the surface where the tag is embedded. For example, the component shown in Fig. 26 has a thickness of 15cm. According to the regulations of the PCI[26] and NPCA[24], the thickness of prefabricated wall components generally ranges from 100mm to 300mm. Therefore, we conducted experiments on components with two different thicknesses: 15cm and 30cm, with the tags embedded at a depth of 3cm in both cases. As Fig. 23 shows, the 30cm thick components exhibit larger location errors and greater variance. We attribute this to the increased multipath effects within thicker components.

5.4 Case Study

Distinguish multiple tags. Our system can not only localize the RFID tag, the key of our system is to accurately distinguish the position of different components. In Tab. 1, we have listed 9 types of components. Their widths and heights mostly range from 50 cm to several meters. Some components, such as beams and columns, have narrower widths. However, these components are typically spaced further apart, making them easier to distinguish compared to

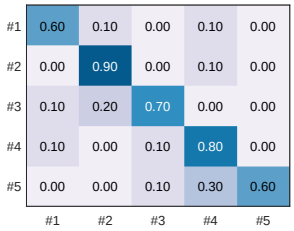

(a) 50cm spacing.

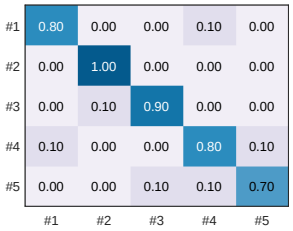

(b) 100cm spacing.

Figure 24: Distinguish multiple concrete components.

panels and slabs. To demonstrate the system's effectiveness in practical scenarios, we use 5 concrete components, labeled from #1 to #5, with a horizontal spacing of 100 cm. Their positions are $[H, W, L] = [1.65m, -1m, 1.5m]$, $[1.65m, 0m, 1.5m]$, $[1.65m, 1m, 1.5m]$, $[0.85m, -0.5m, 1.5m]$, $[0.85m, 0.5m, 1.5m]$. Additionally, we repeated the experiment with a reduced horizontal spacing of 50 cm. As shown in Figure 24, the results indicate that the average distinction accuracy at a 50 cm spacing is 70%, while at a 100 cm spacing, it is 84%. The improvement with 100cm spacing is not substantial because, at the larger spacings, tags nearly move out of the antenna's field of view, leading to a lower SNR (signal-to-noise ratio).

Different user operators. In this section, we evaluate the impact of operational behavior on the experiment. We recruited 9 volunteers and allowed them to move the handheld device in any manner they preferred, such as using their right or left hand, and varying the moving speed, distance, and direction. Each volunteer is required to move the antenna 5 times in 10 seconds and keep the operational behavior the same at each time. Moreover, the volunteers are required to keep the antenna plane facing forward so that the tags can be read. We place the component at $[H, W, L] = [1m, 0m, 1.5m]$ and the location of the user is at $[H, W, L] = [1m, 0m, 0m]$. In this group of experiments, user #5 and #8 move the antenna in a square shape perpendicular to the wall, user #1, #7 and #9 move the antenna in a circle shape, while user #2, #3, #4 and #6 move the antenna in the shape of different polygons. Result in Fig. 25 shows that with most of the operators, RFinder can achieve an average AoA accuracy within

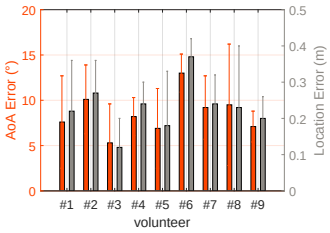

Figure 25: Case study of different user operators.

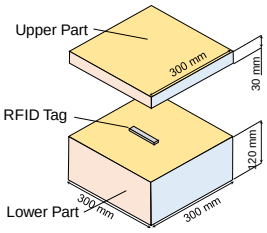

Figure 26: Component structure.

10°. It is also worth noting that with volunteer #3, RFinder achieved the lowest location error. We observed that this volunteer moved the antenna at a faster speed and within a smaller range, compared to the others. So this result aligns with our findings from previous experiments.

6 RELATED WORK

As one of the commonest backscatter technologies [17, 18], RFID has been extensively studied over the years, especially for localization applications. Due to the limited spatial resolution of RFID signal, traditional RFID localization achieves only decimetre or meter scale accuracy. Some recent efforts[11, 33, 41] have been made to achieve more fine-grained localization. A core of those methods is to refine the localization by combining multiple sources of information, *e.g.*, signals collected by different antennas[6], from different spatial locations[3, 23, 32], on different frequencies[42], etc. Although these methods achieve cm-level or even mm-level accuracy, they incur either unacceptable cost or restrictive assumptions on the targets, which makes them unsuitable for our scenarios.

For example, to achieve the fine-grained localization, some systems measure the signal phase at multiple antennas, and use the phased antenna array model to estimate the AoA. Although these techniques improve localization accuracy, they are too bulky to be deployed on portable devices.

To avoid costly antenna arrays, an alternative method is to mount the reader on a robot, and leverage the robot's movement to emulate an antenna array. However, these methods require moving the robot on well-defined trajectories, making them ill-suited for handheld human mobility.

To solve the above problem, some recent works propose handheld RFID localization methods, which achieve fine-grained localization using only one antenna. For example, [12] proposes a portable RFID localization system which leverage user's mobility to emulate an antenna array for fine-grained localization. However, this method requires the user to move his/her hand along a pre-defined trajectory (*e.g.*, a circle). A slight deformation of the trajectory (which is inevitable for human operation) may seriously affect the localization accuracy, which makes the system hard to use in practice. Similar to RFinder, [34] also proposes a portable RFID localization method which achieves single-antenna localization by combining the RFID signal and the IMU signal. However, in this case, the IMU is utilized to calculate the movement distance of handheld devices, which is prone to be affected by the acceleration drift of IMU sensors.

The most relevant work to ours is [25], which designs an RFID localization method for handheld readers. However, it does not consider the practical issues and uses raw accelerations to match the RFID acceleration, which reduces the accuracy because accelerations are much more sensitive to the user's motion.

7 CONCLUSION

This paper introduces RFinder, the first to demonstrate a portable RFID localization system that can estimate the AoA of a tag that is embedded in prefabricated buildings. Through experiments, we show that RFinder achieves an average AoA estimation error of about 11° in the range of 2.5m and a location error at decimeter-level, which is sufficient for distinguishing the prefabricated components.

However, RFinder is not without limitations. First, the reading distance of the embedded RFID tag is restricted to less than 3 meters, making it challenging to localize components on higher walls. This issue can be addressed by using active RFID tags, which offer a longer reading distance. Additionally, we require users to operate the system with the antenna plane facing towards the wall. Since the antenna has a specific FoV, tags outside this FoV will not be read.

Despite these limitations, RFinder also enables multiple applications. For instance, in retail stores, handheld devices can assist clerks in locating misplaced items. Handheld devices can also help medical personnel quickly scan and locate medications, ensuring that storage and distribution comply with safety regulations.

ACKNOWLEDGMENTS

We thank our anonymous shepherd and reviewers for their insightful comments. We are grateful to Mr. Yongjun Zheng (Zhejiang Nayuan Information Technology Co., Ltd.) for providing the application-specific information to this study. This work is supported in part by the National Natural Science Foundation of China (No. 62425207, No. U21B2007, No. 62202264, No. 62394344 and No. 62272293).

REFERENCES

[1] ADSI. 2021. Accident. https://ncrb.gov.in/sites/default/files/ADSI-2021/adsi2021_Chapter-1-Accidents.pdf. (2021).
[2] Amazon. 2023. Impinj R420 Reader. https://www.amazon.com/Impinj-Speedway-Revolution-R420-Reader/dp/B00JPORPE6. (2023).

[3] Zhenlin An, Qiongzheng Lin, Lei Yang, Yi Guo, and Ping Li. 2022. Localizing RFIDs in Pixel Dimensions. *ACM ToSN* 19, 1 (2022), 1–24.

[4] apple. 2024. Apple AirTag. https://www.apple.com/airtag/. (2024).

[5] Caroline Silva Araújo, Leandro Cândido de Siqueira, Emerson de Andrade Marques Ferreira, and Dayana Bastos Costa. 2020. Conceptual Framework for Tracking Metallic Formworks on Construction Sites Using IoT, RFID and BIM Technologies. In *Proceedings of Springer ICCCBE*.

[6] Salah Azzouzi, Markus Cremer, Uwe Dettmar, Rainer Kronberger, and Thomas Knie. 2011. New Measurement Results for the Localization of UHF RFID Transponders Using an Angle of Arrival (AoA) Approach. In *Proceedings of IEEE RFID*.

[7] BIM. 2024. BIM. https://en.wikipedia.org/wiki/Building_information_modeling. (2024).

[8] Tara Boroushaki, Maisy Lam, Laura Dodds, Aline Eid, and Fadel Adib. 2023. Augmenting Augmented Reality with Non-Line-of-Sight Perception. In *Proceedings of USENIX NSDI*.

[9] Jason L Brchan, Lianlin Zhao, Jiaqing Wu, Robert E Williams, and Lance C Pérez. 2012. A real-time RFID localization experiment using propagation models. In *Proceedings of IEEE RFID*. IEEE, 141–148.

[10] Michael Buettner and David Wetherall. 2008. An Empirical Study of UHF RFID Performance. In *Proceedings of ACM MobiCom*.

[11] Alice Buffi, Daniele Fontanelli, David Macii, Valerio Magnago, Andrea Motroni, Paolo Nepa, and Bernardo Tellini. 2019. UHF-RFID Localization: The Problem of Antenna Phase Center in Phase-based Methods. In *Proceedings of IEEE EuCAP*.

[12] Aristidis Raptopoulos Chatzistefanou, Anastasios Tzitzis, Spyros Megalou, George Sergiadis, and Antonis G Dimitriou. 2022. Target Localization by Mobile Handheld UHF RFID Reader and IMU. *IEEE Journal of Radio Frequency Identification* 6 (2022), 426–438.

[13] J Davis, Y Huang, SG Millard, and JH Bungey. 2003. Determination of Dielectric Properties of Insitu Concrete at Radar Frequencies. *Non-Destructive Testing in Civil Engineering* (2003).

[14] designingbuildings. 2024. C30 concrete. https://www.designingbuildings.co.uk/wiki/Common_arrangement_of_work_sections_classification. (2024).

[15] Laura Dodds, Isaac Perper, Aline Eid, and Fadel Adib. 2023. A Handheld Fine-Grained RFID Localization System with Complex-Controlled Polarization. In *Proceedings of ACM MobiCom*.

[16] ebay. 2023. WHEELTEC N200 IMU. https://www.ebay.com/itm/115079020558. (2023).

[17] Xiuzhen Guo, Yuan He, Zihao Yu, Jiacheng Zhang, Yunhao Liu, and Longfei Shangguan. [n. d.]. RF-transformer: a unified backscatter radio hardware abstraction. In *Proceedings of ACM MobiCom*. 446–458.

[18] Xiuzhen Guo, Yuan He, Jiacheng Zhang, Yunhao Liu, and Longfei Shangguan. 2024. Towards Programmable Backscatter Radio Design for Heterogeneous Wireless Networks. *IEEE/ACM Transactions on Networking* (2024).

[19] T. Instruments. 2005. ISM-Band and Short Range Device Regulatory Compliance Overview. https://www.ti.com/lit/an/swra048/swra048.pdf. (2005).

[20] Chengkun Jiang, Yuan He, Songzhen Yang, Junchen Guo, and Yunhao Liu. 2019. 3D-OmniTrack: 3D Tracking with COTS RFID Systems. In *Proceedings of ACM/IEEE IPSN*.

[21] Elia Leoni, Amy L Murphy, and Elisabetta Farella. 2022. Poster: Evaluating RFID for Automatic Checkout in Smart Retail. In *Proceedings of EWSN*.

[22] Yunfei Ma, Nicholas Selby, and Fadel Adib. 2017. Minding the Billions: Ultra-wideband Localization for Deployed RFID Tags. In *Proceedings of ACM MobiCom*.

[23] Andrea Motroni, Paolo Nepa, Valerio Magnago, Alice Buffi, Bernardo Tellini, Daniele Fontanelli, and David Macii. 2018. SAR-based Indoor Localization of UHF-RFID Tags via Mobile Robot. In *Proceedings of IEEE IPIN*.

[24] npca. 2024. npca. https://precast.org/. (2024).

[25] Andreas Parr, Robert Miesen, Fabian Kirsch, and Martin Vossiek. 2012. A Novel Method for UHF RFID Tag Tracking Based on Acceleration Data. In *Proceedings of IEEE RFID*. 110–115.

[26] pci. 2024. PCI. https://www.pci.org/. (2024).

[27] SEIKO RFID. 2023. SEIKO RFID Tag. https://www.seikorfid.com/product/Concrete-Embedded-RFID-Tags.html. (2023).

[28] RFID4U. 2023. TSL 1128 Reader. https://rfid4ustore.com/tsl-1128-bluetooth-uhf-handheld-rfid-reader/. (2023).

[29] RFIDHY. 2023. RFID Concrete TAG. https://www.rfidtaghy.com/product/rfid-concrete-and-construction-tag/. (2023).

[30] A Sattineni. 2008. Real-time management in a BIM model with RFID and wireless tags. *Auburn University* (2008), 67–75.

[31] Longfei Shangguan and Kyle Jamieson. 2016. The Design and Implementation of a Mobile RFID Tag Sorting Robot. In *Proceedings of ACM MobiSys*.

[32] Longfei Shangguan, Zheng Yang, Alex X Liu, Zimu Zhou, and Yunhao Liu. 2015. Relative Localization of RFID Tags using Spatial-Temporal Phase Profiling. In *Proceedings of USENIX NSDI*.

[33] Longfei Shangguan, Zimu Zhou, and Kyle Jamieson. 2017. Enabling Gesture-based Interactions with Objects. In *Proceedings of ACM MobiSys*.

[34] Kaumudi Singh, DN Tejeshwini, Sanmay Patel, Sourav Sudhir, Zuhaib M Ahmed, TV Prabhakar, and Joy Kuri. 2020. Localization of Life Safety Vests in an Aircraft Using Backscattering RFID Communication. *IEEE Journal of Radio Frequency Identification* 4, 3 (2020), 234–245.

[35] Atlas RFID Store. 2023. Laird S9025PR antenna. https://www.atlasrfidstore.com/laird-s9025pr-s8655pr-rhcp-outdoor-rfid-antenna-fcc-etsi/. (2023).

[36] Jue Wang and Dina Katabi. 2013. Dude, Where's My Card? RFID Positioning That Works with Multipath and Non-Line of Sight. In *Proceedings of ACM SIGCOMM*.

[37] Jue Wang, Deepak Vasisht, and Dina Katabi. 2014. RF-IDraw: Virtual Touch Screen in the Air Using RF Signals. In *Proceedings of ACM SIGCOMM*.

[38] Ju Wang, Jie Xiong, Hongbo Jiang, Xiaojiang Chen, and Dingyi Fang. 2016. D-Watch: Embracing "Bad" Multipaths for Device-Free Localization With COTS RFID Devices. In *Proceedings of ACM CoNEXT*.

[39] Xin Xiao, Xiaojun Jing, Siqing You, and Jian Zeng. 2010. An environmental-adaptive RSSI based indoor positioning approach using RFID. In *2010 International Conference on Advanced Intelligence and Awarenss Internet (AIAI 2010)*. IET, 127–130.

[40] Dianhan Xie, Xudong Wang, and Aimin Tang. 2023. MetaSight: Localizing Blocked RFID Objects by Modulating NLOS Signals via Metasurfaces. In *Proceedings ACM MobiSys*.

[41] Lei Yang, Yekui Chen, Xiang-Yang Li, Chaowei Xiao, Mo Li, and Yunhao Liu. 2014. Tagoram: Real-Time Tracking of Mobile RFID Tags to High Precision Using COTS Devices. In *Proceedings of ACM MobiCom*.

[42] Songzhen Yang, Meng Jin, Yuan He, and Yunhao Liu. 2021. RF-prism: Versatile RFID-based Sensing through Phase Disentangling. In *Proceedings of IEEE ICDCS*.

[43] Junjie Yin, Zheng Yang, Sicong Liao, Chunhui Duan, Xuan Ding, and Li Zhang. 2023. TagFocus: Towards Fine-Grained Multi-Object Identification in RFID-based Systems with Visual Aids. *ACM ToSN* 19, 1 (2023), 1–22.